Multi-channel multiple-source optic disk detection (MIUA) Proceedings

C Mazo[a], E Trucco[b], G England, Y Petillot, J Bell, A Harvey*

[a]Optos Plc, Dunfermline, [b]Heriot Watt University, Edinburgh

Abstract. This paper presents an automatic algorithm to locate the optic disk in images from fundus cameras and scanning laser ophthalmoscopes. The algorithm uses red and green images (multi-channel), and combines geometric and brightness information about optic disk and vessel appearance (multiple-source). Location is first attempted on the red channel by orientation correlation, resulting in frequent success. Failure, detected automatically, triggers a multi-channel search combining brightness and local vessel density, orientation and contrast. We achieved 93% success on the STARE test set, a better performance than [1] and similar or better to algorithms of comparable complexity to ours. We also achieved 98% success with ultra-wide-field-of-view images from an OPTOS Panorama ophthalmoscope.

1 Introduction

We propose a multi-channel, multiple-source approach to OD detection. The location of OD and other retinal landmark (macula, vasculature) is an important step towards the automatic detection of symptoms of important retinal and systemic diseases, most notably glaucoma, age-related macula degeneration, and diabetic retinopathy [2,3]. Diabetes, for example, has an average incidence of 3 to 5% in the UK, and peaks to around 20% in some US areas. Many algorithms have been proposed for OD and vasculature detection in fundus images [1–8], both *per se* and in the context of disease detection: see [1] for a recent, concise review. A serious difficulty is that disease symptoms, lesions, imaging conditions and other factors create a significant range of variations in the appearance of retinal images.

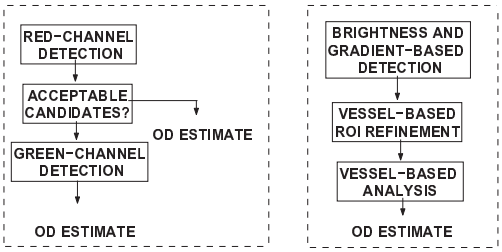

Figure 1. Left: overall system structure. Right: basic structure of green-channel detection.

Most authors have reported algorithms based on single-channel images (typically green), e.g., [1,7,9,10]. Various authors sought to exploit the high brightness or high brightness variation in OD regions, e.g., [4, 11]. Limited performance motivated the use of geometric models [7,9] and vessel geometry [1,10]; see [7] for a concise review of recent work. Knowledge of retinal anatomy has also been used, e.g., in symbolic reasoning [3] and constraint satisfaction schemes [12]. Performance quality is quantified typically by the percentage of true positives (correct detections) in controlled experiments with ground-truth ("gold standard") data. In our system, location is first attempted on the *red* channel by orientation correlation. Although OD brightness does not stand out in red images, the pattern of gradient orientations of contour pixels proves a useful clue resulting in frequent success. Failure, detected automatically, triggers a search on a candidate set of regions of interest (ROIs) identified through both red and green channels. The final detection is based on several properties of candidate ROIs, incl. high brightness and shape, and of blood vessels, incl. density, orientation and contrast. The main contribution of this paper is an efficient and effective combination of multiple information sources within a multi-channel framework. Our implementation achieved 92.5% correct detection on the standard STARE set [13], significantly better than the 86% reported in [1], and 98% correct detection with 219 UWFV images (200° field of view) from a non-mydriatic OPTOS Panorama scanning laser ophthalmoscope (SLO). The remainder of this paper describes briefly our current system and its key modules (Section 2) and some experimental results with the two sets of retinal images (Section 3). We summarize our results in Section 4.

*Christophe Mazo[cmazo@optos.com],Emanuele Trucco [E.Trucco@hw.ac.uk]

2 The algorithm

2.1 System structure

The architecture of the algorithm is shown in Figure 1 (left). First, fundus-camera images are masked to discard the non-data pixels (dark periphery). Detection is then attempted on the red channel only, using shape and brightness information. If the candidate region resulting does not pass an acceptance test, a multi-channel search is triggered (Figure 1 right). Each component is described briefly below.

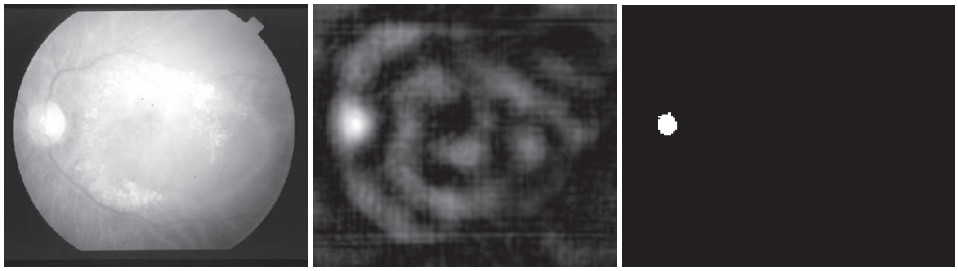

Figure 2. Left: red-channel image. Centre: result of orientation correlation filter. Right: thresholded correlation image (correct detection).

2.2 Red-channel detection and acceptance test

Background elimination. Various solutions are possible given the characteristic circular pattern of fundus camera images. Simply keeping the 0.7% brightest pixels after applying morphological dilation (Intensity maximum, 5-pixel radius) worked very well on STARE images. We found that pushing contour accuracy (e.g., circle detection) did not improve the overall detection quality. *OD candidate selection.* Healthy OD do not appear necessarily brighter than other areas in the red image, but have a well-defined, elliptical shape. The intensity gradient at boundary points is distributed accordingly. We therefore perform orientation correlation on gradient directions with a pre-defined radial pattern of radius 60 pixels (Figure 2). This simple procedure identified the correct candidate quickly in 52.8% of the STARE images (47 out of 81).

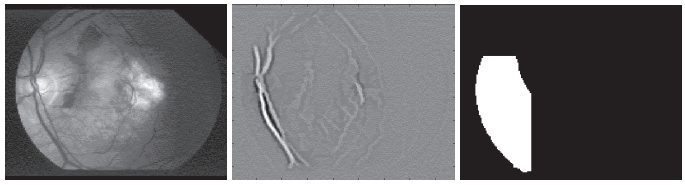

Figure 3. Left: green-channel image. Centre: result of morphological vessel enhancement filter. Right: search region as union of neighborhoods of maximum-response, near-vertical vessel pixels.

Acceptance test. We identify points in likely OD regions as the N highest-response points in the filtered image. N number is determined empirically from experiments on images of the target type (sensor); e.g., $N = 100$ for STARE and OPTOS images. The correct candidate is expected to generate a dense, small cluster of high-response pixels (Figure 2). If this is the case, the algorithm returns the cluster as the final answer, otherwise a multi-channel search is triggered. In detail, the test seeks a high-response pixel $\mathbf{p}_c$ surrounded by a cluster $C_R = \{\mathbf{p}\}$, $\mathbf{p}$ a high-response pixel, which is dense in the sense that $avg(\|\mathbf{p} - \mathbf{p}_c\|) < 10$ pixels and $stdev(\|\mathbf{p} - \mathbf{p}\|) < 3$. The numerical values are related to the size of the OD observed in fundus-camera images; tests indicate that reasonably small variations of these values do not degrade detection performance. Notice that varying N reasonably around 100 makes the candidate cluster slightly smaller ($N < 100$) or introduces a few spurious candidates dropped by subsequent processing ($N > 100$), without worsening the overall performance.

2.3 Multi-channel detection

If OD detection on the red channel fails, the multi-channel detection is triggered. The algorithm structure is shown in Figure 1 (right). In essence, a set of candidate regions is formed using brightness and gradient information. The set is then refined using vessel-related properties. A merit coefficient, c, combining vessel and brightness properties is evaluated for each surviving candidate region. The final OD location is the region maximizing c. Brief details are given below.

Brightness and gradient-based ROI selection. As the OD *may* appear usually as a bright region in the green image, the brightest pixels are located in the green channel and subjected to the grouping test described above, yielding a set C_G. $C = C_G \bigcup C_R$ is the new set of candidates for the multi-channel stage. *Vessel-based ROI pruning.* The candidate set, C, is pruned exploiting vessel-related knowledge. The OD region is expected to be traversed by prominent, mostly vertical vessels, generating strong contours. Morphological vessel enhancement is therefore employed to identify strong vessels in each candidate region [8]. Vessel segments forming angles larger than $30°$ with the image y axis are discarded. Such regions of interest (ROIs) are created around the surviving vessels pixels by overlapping rectangular windows slightly larger than the expected OD size (see above). An example is shown in Figure 3. *Estimating the OD location.* We quantify edge pixel properties within each ROI by running a Canny edge detector ($\sigma = 1$, low threshold = 0.08, high threshold = 0.2). The correct OD region is expected to contain a significant proportion of high-contrast edge pixels with orientations clustering around the image vertical axis. For the k-th ROI, R_k, we compute $c_k = \sum_{\mathbf{p} \in R_k} \|\nabla I(\mathbf{e})\|$, with $\mathbf{e}$ a Canny edge point. This criterion increases with gradient strength and the number of edge points in the ROI, where $\nabla I(\mathbf{p})$ is computed at near-vertical pixels only. The final OD location is $R^* = \arg\max_k \{c_k\}$, a very modest effort given the small number of candidates.

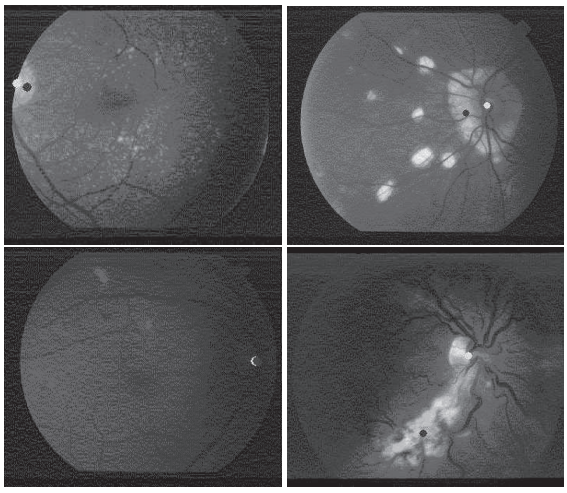

Figure 4. Left column: examples of image classified correctly by our system but not by Hoover and Goldbaum (images 13, 41). Right column: *vice versa* (images 10, 43). White spot is ground truth, black spot estimate.

3 Experimental results

MATLAB and C implementations on a 3-GHz Pentium PC were tested with fundus camera and SLO image sets. We report and discuss our results after stating our criteria for correct detection. *Defining "correct detection".* To compare results meaningfully, we use Hoover and Goldbaum's definition [1]: a correct estimate is a point falling within one average OD radius of the ground-truth location. In all test images the ground truth was established manually by a non-clinician person, and the average radius computed from circles fitted manually to the OD.

Fundus camera tests. Hoover's popular test set [13] contains 605×700 images of 31 healthy and 50 diseased retinas, acquired by a Topcon TRV-50 fundus camera with $35°$ field of view. The author's method [1] is reported to fail on 9 images (89% success). Our system failed on only 6 images (93% success), namely 10, 19, 20, 27, 43, 44, and succeeded on 6 of the 9 misclassifications by Hoover's method, namely 3, 7, 13, 26, 41, 139. All of these but 26 were classified correctly by the simple red-channel module, and no multi-channel detection was necessary. The reason is arguably that vessel direction as estimated in [1] does not give enough information when only part of the vasculature is visible; instead, we use vessel *density* in the final merit coefficients, making classification more

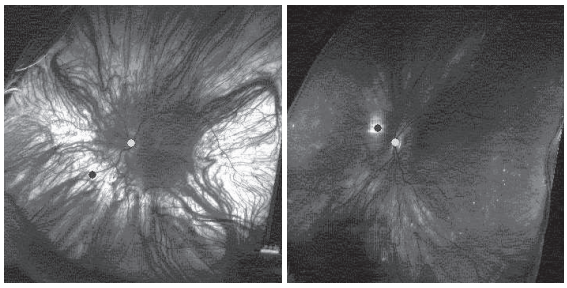

Figure 5. Examples of UWFV images classified incorrectly due to severe retina alterations (left) and imaging conditions (right, strong reflection). White spot is ground truth, black spot estimate.

reliant to vasculature occlusion. Figure 4 shows examples of images on which we succeed and [1] fails and *vice versa*. This solution is simpler than Foracchia's *et al.* parametric model of vessel geometry [10], who report 98% success on the STARE set. They report difficulties with images 8, 26, 27, 41; interestingly, our system succeeded on all but one (27). Indeed our MATLAB prototype ran in 4 s on average (the C++ one in 0.4 s), significantly faster than the 2 minutes reported by Foracchia's MATLAB system on a 2-GHz Pentium PC even considering the different clocks. *UWFV images*. We also tested the system with 219 1984×1984 images of 110 healthy and 109 diseased retinas, acquired by a non-mydriatic OPTOS Panorama200 SLO with up to 200° field of view. Our systems failed on only 5 images (98% success) severely departing from normal retina appearance due to diseases or lesions, or with imaging artifacts. Some examples are shown in Figure 5.

4 Conclusions

We have presented a multi-channel, multiple-source OD detection algorithm. The strength of the approach is the combination of multiple-channel information with multiple sources of evidence, incl. vessel density, orientation and contrast, and gradient orientation at OD contour pixels. Current results show very good performance with the standard STARE test set as well as with 219 ultra-wide field of view SLO images. An important goal of our current and future work is the development of a computer-assisted screening system, aimed to increase early detection of symptoms of high-incidence diseases (e.g., diabetes).

References

1. A. Hoover & M. Goldbaum. "Locating the optic nerve in a retinal image using the fuzzy convergence of the blood vessels." *IEEE Trans. Medical Imaging* **22(8)**, pp. 951–8, 2003.
2. A. Can, H. Shen, J. N. Turner et al. "Rapid automatic tracing and feature extraction from retinal fundus images using direct exploratory algorithms." *IEEE Trans. Information Technology in Biomedicine* **3(3)**, pp. 125–138, 1999.
3. A. Pinz, S. Bernogger, P. Datlinger et al. "Mapping the human retina." *IEEE Trans. Medical Imaging* **17(4)**, pp. 606–619, 1998.
4. S. Chauduri, S. Chatterjee, N. Katz et al. "Automatic detection of the optic nerve in retinal images." In *Proc. IEEE Int.Conf. on Image Processing*, pp. 1–5. 1989.
5. A. Can, C. Stewart, B. Roysam et al. "A feature-based robust hierachical algorithm for registering pairs of images of the human retina." *IEEE Trans. Pattern Analysis and Machine Intelligence* **24(3)**, 2002.
6. X. Jiang & D. Mojon. "Adaptive local thresholding by verification-based multithreshold probing with an application to vessel detection in retinal images." *IEEE Trans. Pattern Analysis and Machine Intelligence* **25(1)**, pp. 131–7, 2003.
7. H. Li & O. Chutatape. "Automated feature extraction in color retinal images by a model based approach." In *IEEE Trans. Biomedical Engineering*, volume 51, pp. 246 – 254. 2004.
8. F. Zana & J.-C. Klein. "Segmentation of vessel-like patterns using mathematical morphology and curvature evaluation." *IEEE Trans. Image Processing* **10(7)**, pp. 1010–1019, 1998.
9. L. Lowell, A. Hunter, D. Steel et al. "Optic nerve head segmentation." *IEEE Trans. Medical Imaging* **23(2)**, 2004.
10. M. Foracchia, E. Grisan & A. Ruggeri. "Detection of optic disc in retinal images by means of a geometrical model of vessel structure." *IEEE Trans. Medical Imaging* **23(10)**, pp. 1189 – 1195, 2004.
11. C. Sinthanayothin, J. F. Boyce, H. L. Cook et al. "Automated localization of the optic disc, fovea, and retinal blood vessels from digital color fundus images." 1999.
12. E. Trucco & P. J. Kamat. "Locating the optic disk in images via plausible detection and constraint satisfaction." 2004.
13. S. data. "www.parl.clemson.edu/stare/nerve/."